PCCP

Accepted Manuscript

ROYAL SOCIETY OF CHEMISTRY

www.rsc.org/pccp

Physical Chemistry Chemical Physics
CREATED USING THE RSC LaTeX PCCP ARTICLE TEMPLATE – SEE www.rsc.org/electronicfiles FOR DETAILS
ARTICLE TYPE
www. rsc.org/xxxxxx | XXXXXXXX

Interface structure and reactivity of water-oxidation Ru-polyoxometalate catalysts on functionalized graphene electrodes.†

Changru Ma,[*a‡] **Simone Piccinin,**[b,a] **and Stefano Fabris**[b,a]

Received Xth XXXXXXXXXX 20XX, Accepted Xth XXXXXXXXX 20XX
First published on the web Xth XXXXXXXXXX 200X
DOI: 10.1039/b000000x

We combine classical empirical potentials and density functional theory (DFT) calculations to characterize the catalyst/electrode interface of a promising device for artificial photosynthesis. This system consists of inorganic Ru-polyoxometalate (Ru-POM) molecules that are supported by a graphitic substrate functionalized with organic dendrimers. The experimental atomic-scale characterization of the active interface in working conditions is hampered by the complexity of its structure, composition, as well as by the presence of the electrolyte or solvent. We provide a detailed atomistic model of the electrode/catalyst interface and show that the catalyst anchoring is remarkably dependent on water solvation. A tight host-guest binding geometry between the surface dendrimers and the Ru-POM catalyst is predicted in vacuum conditions. The solvent destabilizes this geometry, leads to unfolding of the dendrimers and to their flattening on the graphitic surface. The Ru-POM catalyst binds to this organic interlayer through a stable electrostatic link between one POM termination and the charged terminations of the dendrimers. The calculated dynamics and mobility of the Ru-POM catalyst at the electrode surface are in fair agreement with the available high-resolution transmission electron microscopy data. In addition, we demonstrate that the high thermodynamic water-oxidation efficiency of the Ru-POM catalyst is not affected by the binding to the electrode, thus rationalizing the similar electrochemical performances measured for homogeneous and heterogeneous Ru-POM catalysts.

1 Introduction

The sunlight-driven oxidation of water into protons and molecular oxygen is a central process in the solar-to-chemical energy conversion [1,2]. This reaction represents a bottleneck for the development of new artificial photosynthesis devices. [3–5] The electrochemical light-induced water oxidation is a four-electron process that requires a free energy of 4.92 eV, equivalent to a potential of 1.23 V (referenced to the normal hydrogen electrode, NHE, and at pH 0). Suitable catalysts are needed to promote this reaction minimizing the thermodynamic losses, i.e. the overpotential. These active materials need to be in contact with the electrode and will therefore operate as heterogeneous catalysts. The most efficient examples are based on precious metal oxides, like RuO_2 and IrO_2, but significant progress has been recently made in replacing the metal cations with earth-abundant elements such as Co, Ni and Mn [6–8]. The surfaces of these materials display complex morphologies exposing a wide variety of possible active sites (steps, kinks, point defects, etc). This hampers the identification of clear structure-function relationships that are necessary for a rational catalyst engineering.

An alternative approach consists in anchoring molecular catalysts to the electrodes. This requires devising specific binding mechanisms that do not degrade the catalytic efficiency of the molecular complexes in the homogeneous phase. Toma and coworkers have recently achieved this important goal by successfully anchoring a fully inorganic Ru-based polyoxometalate (Ru-POM) complex to a conductive graphitic substrate [9]. The Ru-POM molecule is formed by a tetraruthenium-oxo core $[Ru_4O_4(OH)_2{\cdot}(H_2O)_4]^{6+}$ sandwiched by two POM $[SiW_{10}O_{36}]^{8-}$ units, and promotes water oxidation with low over-potential (0.35 V), high turn over frequency ($>$ 450 cycles per hour) and no deactivation [10,11]. It is among the best catalysts for water oxidation reported to date. Its working mechanisms in the homogeneous phase have recently been disclosed by means of density functional theory (DFT) calculations [12,13].

The device fabricated by Toma and coworkers comprises multiwalled carbon nanotubes (MWCNT) functionalized with organic polyamidoamine ammonium dendrimers (MWCNT-

† Electronic Supplementary Information (ESI) available. See DOI: 10.1039/b000000x/

[a] *SISSA, Scuola Internazionale Superiore degli Studi Avanzati, Via Bonomea 265, 34136 Trieste, Italy; E-mail: changru.ma@epfl.ch*
[b] *CNR-IOM, Istituto Officina dei Materiali, Centro DEMOCRITOS, Via Bonomea 265, 34136 Trieste, Italy*
‡ Present address: Institute of Theoretical Physics, C3PN, École Polytechnique Fédérale de Lausanne (EPFL), CH-1015 Lausanne, Switzerland

dend), which bind the Ru-POM molecular catalyst (Fig. 1). The functionalized MWCNTs, deposited on a conducting substrate, provide a heterogenous support for the Ru-POM complex, which maintains its molecular structure, and facilitates the sequential electron transfer to the electrode driven by the electric potential. Quintana *et al.*[14] recently showed that the same approach can be applied to anchor Ru-POM to graphene as well, obtaining a similar catalytic performance, with no sign of degradation and with an an overpotential as low as 300 mV at neutral pH.

The dynamics of the Ru-POM molecule on functionalized graphene was recently studied by Ke *et al.*[15] by employing time-resolved high-resolution transmission electron microscopy (HRTEM). These measurements showed that, at room temperature, individual Ru-POM molecules can explore various binding geometries, while the in-plane mobility is limited to a window of $\pm$ 2 Å around the anchoring point. We remark that such HRTEM measurements are very challenging and require high-vacuum conditions. This is a case where numerical materials modeling can provide complementary insight by clarifying the effects of the electrolyte on the binding and mobility of the catalyst to the catalyst.

In this work we employ classical interatomic potentials to characterize the atomistic structure of the Ru-POM/electrode interface, while ab-initio DFT calculations are used to address the thermodynamics of the water-oxidation reaction. We show the important effects of the electrolyte on the binding geometry of the Ru-POM catalyst to the electrode. The simulations allow us to elucidate the role of electrostatics in the catalyst/electrode interaction and to rationalize the transposition of the Ru-POM high catalytic efficiency from the homogeneous into the heterogeneous phase.

2 Methods

We employ two simulations approaches. The first one aims at characterizing the structure of the active interface formed by the functionalized graphitic support and the molecular Ru-POM catalyst. The complexity of this heterogeneous system (Ru-POM, MWCNT/graphene, dendrimers) (Fig. 1) together with the presence of the solvent require the use of classical potentials. The second approach characterizes the electronic properties of the system by means of ab-initio DFT methods. These approaches are also used to calculate the thermodynamics of the electrochemical water-oxidation promoted by the Ru-POM anchored at the electrode.

2.1 Empirical force field calculations

Our strategy to determine and to validate the empirical force field is to start modeling accurately the individual components and then treating their mutual interactions. We benchmark our force fields against DFT or Quantum Mechanics / Molecular Mechanics (QM/MM) simulations, where available.

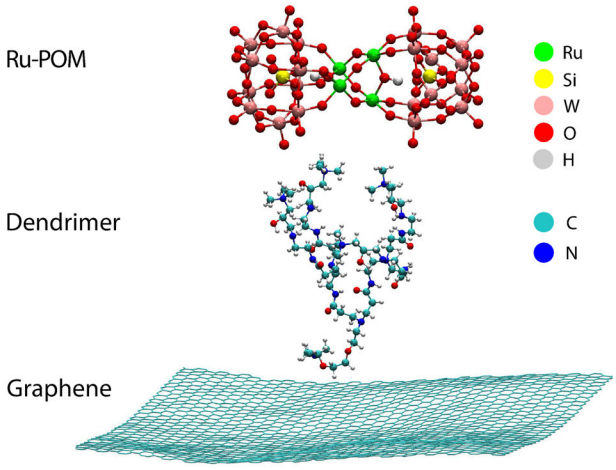

Fig. 1 Geometry of the isolated Ru-POM molecule, of the organic polyamidoamine ammonium dendrimers dendrimer and of the graphene support.

The Ru-POM complex (upper panel of Fig.1) was described as a rigid body consisting of point charges, which were fitted to the DFT-PBE electron density by using the densities and derived atomic point charges (DDAP) method of Bloechl[16]. We found O atoms belonging to the POM terminations to have an average charge of -0.914, while those belonging to the Ru_4O_6 core have a charge of -0.902. Given the similarity of the two values we decided to treat all O atoms as having the same charge of -0.912. Similarly, the charges of the other species were set to the average over all the atoms with the same type.

The graphene substrate was modeled as a (20 $\times$ 30) single layer graphene sheet. The organic polyamidoamine ammonium dendrimers and graphene were modeled using the AMBER force field (GAFF)[17], and water was treated using the modified TIP3P model[18].

Classical molecular dynamics simulations of the whole system (Ru-POM, graphene and dendrimers in solution) are performed at constant pressure (1 bar) and temperature (300 K). We first performed an equilibration run of 5 ns with a time step of 0.5 fs. The production runs were performed in the NVT ensemble for up to 60 ns. These calculations used the LAMMPS Molecular Dynamics Simulator[19] together with the particle-mesh Ewald method for the long-range electrostatics[20]. The non-bonded interaction cutoff was set to 12 Å for all simulations. The cross-term nonbonding Lennard-Jones potential between different types of atoms were obtained through the geometric rule ($\varepsilon_{ij} = \sqrt{\varepsilon_i \varepsilon_j}$, $\sigma_{ij} = \sqrt{\sigma_i \sigma_j}$), with the exception of the Ru - O_{water} interaction, which is supplied directly (see Table SI-1†).

2.1.1 The Ru-POM/water interaction. The interaction between Ru-POM and the rest of the system was described by point-charge electrostatics and through a Lennard-Jones (LJ) potential. In particular, concerning the interaction with water the Lennard-Jones parameters for W were taken from the work of López et al.[21], who studied POMs in solution. For Si, we used the work of Tang *et. al*[22], who modeled silicon nanocrystals in water, and we extracted their LJ parameters for the interaction between 4-fold coordinated Si and O. The LJ parameters for O_{Ru} are assumed to be the same as those for the oxygen in the TIP3P water. The LJ parameters for O_{POM}, on the other hand, are fitted to reproduce our QM/MM results[12], where the catalyst was treated quantum mechanically (DFT-PBE) and the solution was described using the TIP3P model. For the Ru-O_{water} interaction we derived ad-hoc parameters, to correctly describe the bond-length between the Ru cations and their water ligands. All the parameters of the LJ force field to simulate Ru-POM in water are reported in Table SI-1†.

In Fig. 2 we compare the Ru-O_{water} and O_{POM}-H_{water} radial distribution functions obtained using the classical force field and QM/MM simulations, showing an excellent agreement. In the Supporting Information we also show the time evolution of Ru-O_{water} bond lengths comparing the results obtained using the force field and those obtained in QM/MM simulations (Fig. SI-1†).

2.1.2 Graphene/water interaction. We employ parameters from the literature[24,25] shown in Table SI-2†for the carbon atoms in graphene layer. The carbon in graphene sheet is modeled as uncharged sp^2 carbon[26]. Using this parametrization we obtained a lattice parameter of graphene of 2.46 Å, which matches the experimental value. For water, the modified TIP3P model[18] was adopted. This three-site water model has been widely used together with AMBER force fields[24] in evaluating structural properties of various dendrimers in solution[27–29].

Cicero *et al.* investigated water confined between graphene sheets using DFT-PBE simulations[23]. The system they considered included two graphene layers held 25.02 Å apart, and 108 water molecules in a periodically repeated simulation cell. In our classical simulations, at room temperature and zero pressure with periodic boundary conditions, we consider a 20×30 graphene layer surrounded on both sides by water, with a total of 6352 water molecules. The size of the simulation cell is $85.20 \times 32.83 \times 73.79$ Å^3. In Fig. 2(c) we show the density of water molecules computed along the direction perpendicular to graphene surface and a comparison with DFT results[23]. We find no water molecules within the first 2 Å region from the graphene sheet, while the first peak appears around 3.5 Å, with the oxygen peak at slightly lower distance from graphene compared to hydrogen. This is in agreement with DFT results, both in terms of peak positions and height.

2.1.3 Ru-POM/dendrimer interaction. The parameters for the polyamidoamine ammonium dendrimer were drawn from the widely used general AMBER force field (GAFF)[17]. Each dendrimer has four positively charged -$CH_2N(CH_3)_3$ terminations whose charge, +0.93 *e*, was determined by the AM1-BCC method[30].

In order to determine how well our classical force field can describe the interface between dendrimer and Ru-POM molecule, we compare the geometrical properties obtained using our empirical force field with DFT-PBE calculations. For the classical simulations we use a periodic 20×30 model of a graphene layer with either one or two dendrimers chemisorbed on one side, with the anchoring groups positioned 45 Å apart. We considered both the system in the absence and in the presence of the solvent, in the latter case using 13857 water molecules and 2 Na^+ counterions in a period box of dimensions $85.20 \times 69.37 \times 73.79$ Å^3. The LJ parameters for the counter ions are $\varepsilon = 0.0028$ kcal mol^{-1} and $\sigma = 3.3284$ Å. The simulations are carried out at room temperature, in the NVT ensemble.

A single Ru-POM molecule was placed in proximity to the dendrimers and the whole structure was relaxed in the absence of water. For the DFT calculations we considered the relaxed geometry obtained in the classical simulation, and following Li *et al.* and Sun *et al.* [31,32] we replaced the graphene layer with two coronene molecules ($C_{12}H_{24}$), covalently bonded to each of the two dendrimers. The whole structure was then relaxed in gas phase (see Fig. SI-2†). By comparing the final geometries, we find very small structural changes. The most significant are deviations of O_{POM} - $H_{dendrimer}$ distances by less than 0.2 Å. These small discrepancies are most likely due to the lack of Van der Waals interactions in the DFT-PBE calculations.

2.2 DFT Calculations

The electronic structure of the systems is investigated using density functional theory (DFT)[33] calculations, employing the Perdew-Burke-Ernzerhof (PBE) generalized gradient approximation (GGA)[34] for the exchange and correlation functional. We use a plane wave and ultrasoft-pseudopotentials[35] approach as implemented in the Quantum ESPRESSO package[36]. The kinetic energy cutoffs for the plane wave and density expansions are 30 Ry and 300 Ry, respectively. All the structures were fully relaxed using spin-polarized calculations, until all forces on all atoms were less than 0.09 eV/Å and the difference of the total energy between two consecutive geometrical optimization steps was below 2 meV. In the DFT-PBE calculations, coronene molecules were used as models for graphene (see Fig. SI-2†).

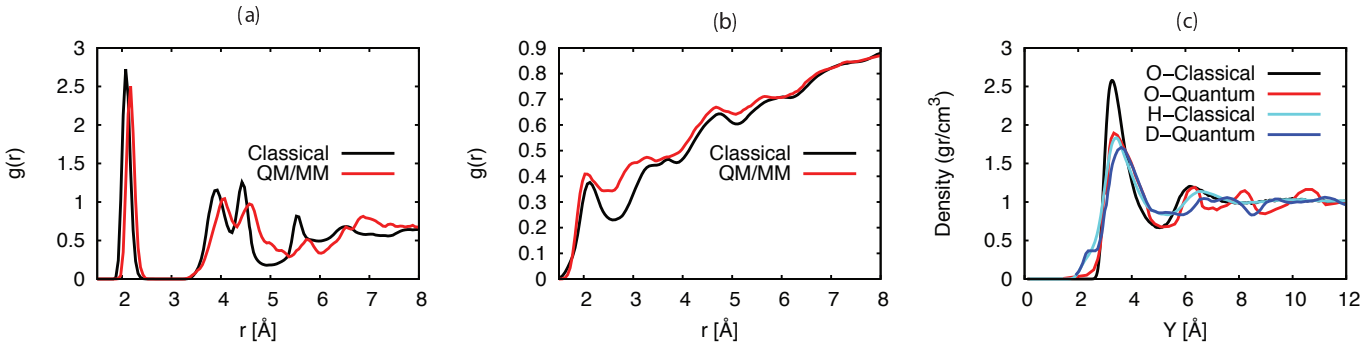

Fig. 2 Calculated classical (black line) and QM/MM (red line) radial distribution functions of the Ru-O_{water} (a), O_{POM}-H_{water} (b) pairs. In panel (c) we show the density of water molecules computed along the direction perpendicular to graphene surfaces. Here the DFT data are taken from the work of Cicero *et al.*[23]

2.3 Calculation of oxidation potentials

To compute the free energy cost of the oxidation steps along the catalytic cycle we employ the protocol proposed by Nørskov *et al.*[37], where all oxidations are considered to be proton-coupled electron transfer (PCET) processes. This approach has been previously applied for water oxidation[38–40] and oxygen reduction[37] reactions on metal, metal oxide surfaces and metal complexes[12,41]. Here we briefly summarize the key concepts.

For a PCET, the chemical potentials of protons and electrons do not need to be known separately. This simplifies the calculations considerably, since the sum of those two chemical potentials is equal to the chemical potential of molecular hydrogen in the gas phase, if all redox potentials are referenced to the Normal Hydrogen Electrode (NHE):

$$\mu(H_2) = 2\mu(H^+) + 2\mu(e^-). \quad (1)$$

At pH=0 and the absence of an external bias, the free energy difference ΔG for a PCET step can be computed as:

$$\Delta G \simeq \Delta E + \Delta ZPE + \Delta H - T\Delta S, \quad (2)$$

where ΔE is the DFT total energies difference, ΔZPE represents the change in zero point energy, ΔH and ΔS are the differences in enthalpy and entropy. The total energy difference ΔE for a PCET process, for example from the initial state S_0 to first intermediate S_1 (see Fig. 5), is calculated as:

$$\Delta E = E(S_1) + \frac{1}{2}E(H_2) - E(S_0) \quad (3)$$

where $\frac{1}{2}E(H_2)$ is half the energy of a hydrogen molecule.

Normal mode analysis was used to calculate ΔZPE, while enthalpy and entropy of gas-phase molecules were obtained from standard thermodynamic tables[42].

3 Structural characterization of the Ru-POM/electrode interface

3.1 Interface structure in vacuum conditions

In this section we describe the binding of Ru-POM to functionalized graphene in the gas phase, i.e. in the absence of the solvent. We remark that the binding geometry and the mobility of the Ru-POM catalyst is likely to depend on the density of the dendrimers. For this reason we start by considering the low density case, in which only one dendrimer is present on the (20×30) graphene supercell. In the initial configuration the Ru-POM is in the gas phase at a distance of 45 Å from the graphene surface. During the first 10 ps of molecular dynamics, the Ru-POM quickly approaches the graphene sheet, while the four branches of the dendrimer tightly embrace it, leading to the characteristic host-guest binding geometry displayed in Fig. 3a. After this transient, the room-temperature MD simulations show that the catalyst remains steadily bound to the dendrimer, as evident from the Ru-POM/graphene distance plotted in Fig. 3b. In this binding configuration, the Ru-POM catalyst displays a fair in-plane mobility, with ≈15 Å fluctuations in the x and y coordinates of the Ru-POM center of mass (Fig. 3c). This mobility originates from the diffusive motion of the dendrimer around its surface anchoring group, and is actually related to the low density of the surface functional groups.

Also when the density of the dendrimers is higher – two dendrimers on the (20×30) graphene supercell – the MD simulations show that the bound configuration is very stable (Fig. 3e), but in this case the binding geometry involves more than one dendrimer. A snapshot of the equilibrated interface structure (Fig. 3d) clearly shows that, for this specific dendrimer distribution, each of the two POM caps of the Ru-POM catalyst interacts with one surface dendrimer. This binding configuration is clearly much more constrained with respect to

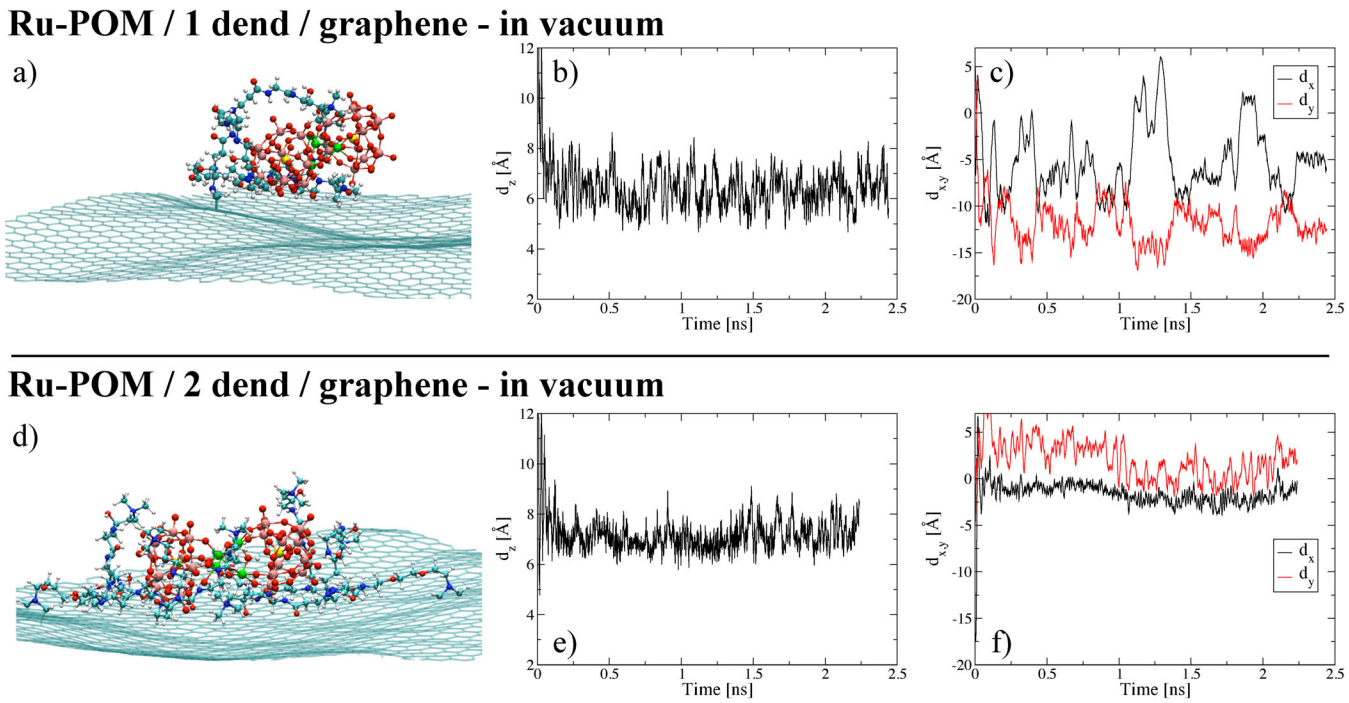

Fig. 3 Molecular dynamics simulation in vacuum at room temperature, with the Ru-POM anchored via either one (a-c) of two (d-e) dendrimers. a) and d) Snapshot of the system in the bound configuration; b) and e) vertical distance d_z between the center of mass of Ru-POM and graphene; c) and f) in-plane displacement d_x and d_y of the center of mass relative to the anchoring point (center of the anchoring points in the 2 dendrimer case).

the low-coverage one because of the presence of two surface anchoring points. The catalyst in-plane mobility is indeed limited to ≈ 4 Å, as displayed in Fig. 3f. The orientation of the main Ru-POM longitudinal axis remained mostly parallel to the graphene plane during the whole MD simulation (2.3 ns).

The experiments by Ke *et al.*[15] show that the in-plane movement of individual Ru-POM molecules is constrained within a $\pm$ 2 Å window in each direction. We note that it is difficult to determine the surface coverage of the dendrimers in the experimental sample. At the same time it is also not possible to explore with the simulation a full spectrum of different dendrimer and catalyst coverages, hence a direct comparison between theory and experiment is problematic. We can however remark that a good agreement between the measured and simulated in-plane Ru-POM mobility ($\approx$ 4Å) is only displayed when the dendrimer coverage is high, namely when more than one dendrimer is involved in the binding of Ru-POM to graphene.

On the basis of the binding energetics we can estimate that electrostatics accounts for 99.3 % and 98.3% of the total binding energy for the Ru-POM in the one- and two-dendrimer geometries, respectively. These contributions comes from the electrostatic interaction between the negatively charged Ru-POM molecule (10−) and the positively charged groups (+1) located at the termination of each of the four branches of both dendrimers.

3.2 Interface structure in the presence of the electrolyte

Solvation of the system in water obviously leads to a considerable screening of the electrostatic interaction. Here we consider the case in which the 20×30 graphene layer is functionalized with two dendrimers. We start the MD simulation with the Ru-POM molecule at a distance of 45 Å from the graphene surface and with water filling all the available space. The evolution of the vertical distance between the Ru-POM center of mass and the graphene sheet is shown in Fig. 4b. At room temperature, within about 10 ns the molecule is attracted by the substrate and remains stably bound to the substrate for the remaining part of the MD simulation (48 ns). A snapshot of the system in the equilibrated bound configuration is shown in Fig. 4a. By comparing the binding geometries in vacuum and in solution, it is clear that the presence of water destabilizes the selective host-guest interaction between Ru-POM and the dendrimer (see vacuum case, Fig. 3d). The solvent leads to a flattening of the functional groups on the graphitic

surface. The catalyst forms a stable link with the organic dendrimers with only one of its two POM caps, while the other remains exposed to the solvent. At variance to the vacuum case, the binding in the presence of the solvent does not involve all the available dendrimers, but only some branches (two in the present case) of one dendrimer.

Once a bound configuration is reached, the distance between the Ru-POM catalyst and the support remains quite constant: The average distance between the Ru-POM center of mass and graphene is 12.5 ± 1.6 Å (the average is taken on the last 48 ns of the simulation, discarding the first 10 ns where the molecule approaches the substrate). In addition, the distance between Ru-POM and dendrimer terminations at the contact link is very stable. This is shown in Fig. 4c, which reports the shortest distance between the Si atom in the POM caps and the N atom of the closest dendrimer termination. At equilibrium (t>25 ns in the Figure), the fluctuations of the catalyst-dendrimer distance are small, within a ±2Å window. On the other hand the center of mass of Ru-POM is quite mobile on the graphene plane, as displayed in Fig. 4d. The position of the Ru-POM center of mass in the x and y planes fluctuates in a ±20Å window, while the axis of the molecule relative to the graphene plane tilts considerably during the simulation (Fig. 4e). This surface mobility of the Ru-POM catalyst reflects the diffusion of the dendrimers on the graphene surface about their anchoring point. In summary, our simulation show that, in solution, the Ru-POM catalyst is stably bound to one/two dendrimer branches via one of its two POM caps, and that the catalyst is fairly mobile on the graphene surface because it is dragged by the dendrimers during their diffusion dynamics.

To explore whether other stable interface structures are stable in solution, we solvated the host-guest binding geometry in vacuum (see Fig. 3d) and used it as the initial configuration for a second MD simulation in solution. Within 30 ns of molecular dynamics at room temperature, the presence of the solvent induced the unfolding of the dendrimers away from the Ru-POM molecule and their flattening on the graphene surface. The equilibrated interface structure obtained from this simulation was comparable to the one described above. As in the previous simulation in solution, the Ru-POM molecule binds to the dendrimer terminations only with one of the two POM caps.

This demonstrates the substantial effect of the solvent on the structure and nature of the catalyst-electrode interface. In vacuum the dendrimers tend to maximize the binding electrostatic interactions by increasing the contact area with the Ru-POM molecule. This leads to the compact host-guest geometry. The polar solvent competes with the dendrimers in terms of interaction with the catalyst. Solvation leads to an overall reduction of the Ru-POM/dendrimers interaction. With respect to the vacuum case, when the catalyst is solvated a considerable

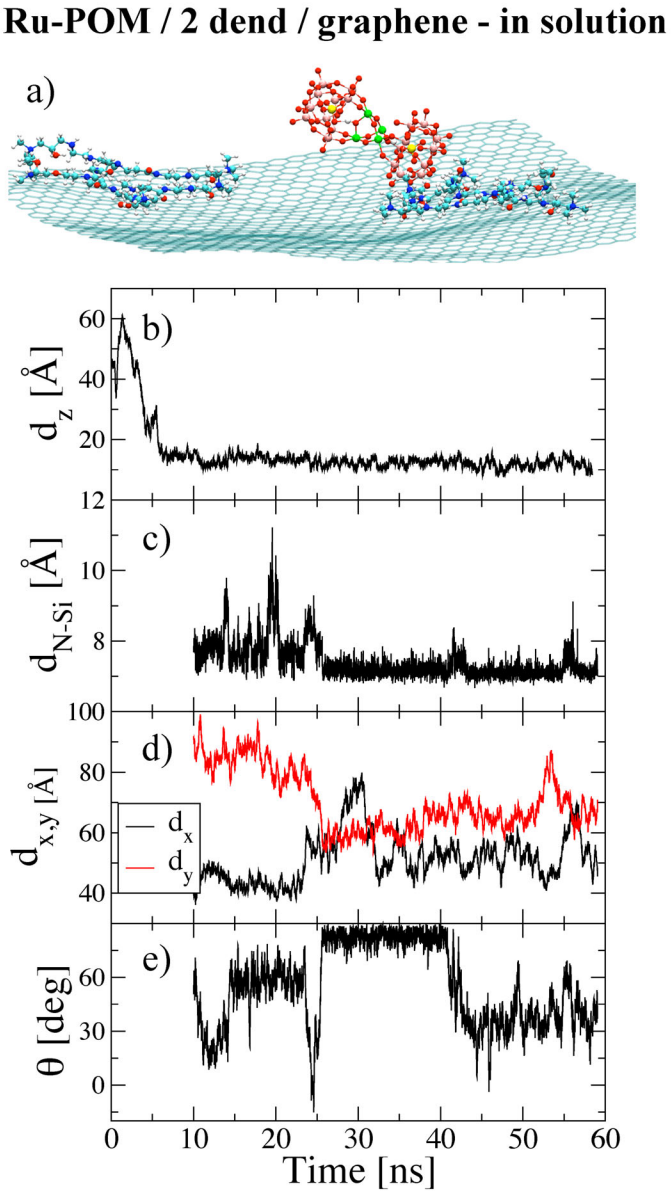

Fig. 4 Molecular dynamics simulation in solution at room temperature: a) Snapshot of the system in the bound configuration (water not shown); b) Distance between the center of mass of the Ru-POM molecule and the graphene layer during a free MD simulation at room temperature; c) Distance between the Si atom at the center of one two POM terminations and the N atom of the closest dendrimer termination; d) In-plane displacement of the center of mass of Ru-POM; e) Angle formed between the longitudinal axis of Ru-POM and the plane of graphene along the same simulation. The last three quantities are monitored only once Ru-POM binds to graphene.

portion of the dendrimers are not anymore in contact with the ionic molecule, which is electrostatically screened by the polar solvent. These dendrimers are therefore free to bind to the graphene substrate by Van der Waals interaction, which is maximized by spreading out on the substrate.

To gain further insights on the strength of the interaction between Ru-POM and functionalized graphene in solution, we computed a histogram of the distance between the center of mass of Ru-POM and graphene along the last 48 ns of the room temperature molecular dynamics. The resulting probability density $P(z)$ as a function of distance is well fitted by a gaussian with a standard deviation $\sigma = 1.6$ Å (see Fig. SI-3†). The free energy profile $F(z) = -k_B T \times log(P(z))$ correspondingly shows a local minimum around the binding geometry, requiring 1.3 kcal/mol for a displacement of $2\sigma = 3.2$ Å away from the minimum (and 2.9 kcal/mol for a displacement of $3\sigma = 4.8$ Å).

Overall, our MD simulations in solution show that the functionalization of graphene with positively charged organic dendrimers leads to the formation of a structure in which the ligands wet the substrate and electrostatically attract the Ru-POM ion. The molecule selectively binds with one POM termination to the dendrimer ends, forming a stable bond. The in-plane mobility of the molecule is a direct consequence of the degree of freedom of the dendrimer branches, which is also dependent on the dendrimer coverage.

4 Reaction intermediates for water oxidation

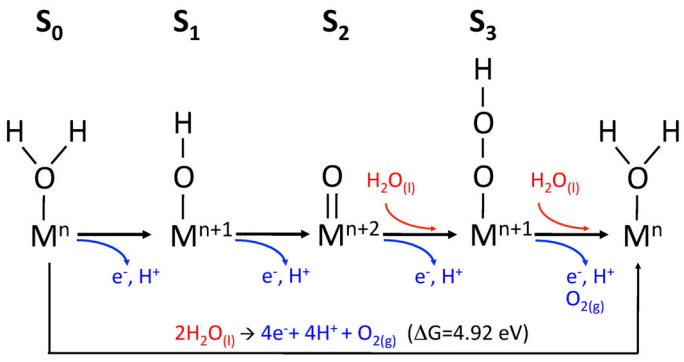

Fig. 5 Water oxidation mechanism modeled in this work.

The water oxidation mechanism promoted by Ru-POM in the homogeneous phase has been analyzed in detail in our earlier publications [12,13]. In this Section, we report the thermodynamics of water oxidation catalyzed by the Ru-POM complex bound to the electrode. We thus determine whether the interaction with the functionalized graphitic support and the resulting electrode-catalyst interface have an effect on the intrinsic catalytic efficiency of the Ru-POM catalyst.

In our previous work we found that the key step, i.e. the formation of the oxygen-oxygen bond, takes place through a nucleophilic attack of a solvent water molecule on a Ru^{VI}=O intermediate. We identified a reaction cycle involving a single Ru metal center, where a sequence of four proton-coupled electron transfer (PCET) reactions leads to the oxidation of two water molecules, the release of molecular oxygen and four electrons and protons. A scheme showing this reaction cycle is presented in Fig. 5.

In the initial state S_0 a water molecule binds to each of the four Ru^{IV} ions. Here we consider a sequence of four PCET steps involving a single Ru ions and its ligands, while the remaining Ru ions keep their oxidation state IV and their water ligand unchanged (Ru^{IV}-OH_2). By comparing the energetics of this reaction cycle *i)* in the homogeneous phase and *ii)* when Ru-POM binds to functionalized graphene, we evaluate the role of the electrode/catalyst interface on the thermodynamics of the process.

In our previous work [12] we have shown that the free energy cost of each PCET is quite sensitive to the choice of the approximation used for the exchange and correlation functional. We showed that the hybrid functionals were necessary for obtaining good agreement with the experimental voltammetry data. Here, however, we aim at determining how the presence of the electrode surface modify the water-oxidation energetics with respect to that one of the Ru-POM homogeneous catalyst. Hence we are not interested in the *absolute* values of the PCET energy costs, but in their *relative* differences with and without the electrode surface. The evaluation of the relative difference does not require the computationally demanding hybrid functionals. In the following, unless otherwise stated, all calculations are performed at the DFT-PBE level.

The structural model adopted to investigate the role of the heterogeneous support is the one shown in Fig. SI-2†. The size of the complete graphene/dendrimer/Ru-POM system is too large for performing DFT calculations. Following other works [31,32], in our DFT calculations we considered a simplified model of the graphitic substrate by replacing the dendrimer/graphene interface with dendrimer-functionalized coronene molecules. This is certainly an oversimplification when studying molecular chemisorption on graphene. [31,32] We remark however that the Ru-POM molecules do not bind directly to the graphitic support, but they are bound to the polyamidoamine ammonium dendrimers, which are in turn supported by the graphitic substrate. Moreover, the local electronic structure of the central C atoms in the coronene molecule is in good agreement with the electronic structure of an extended graphene sheet. As a result, describing the Ru-POM/dendrimer interaction by replacing the 2D graphitic support with a polycyclic aromatic hydrocarbon can be consid-

ered an adequate simplified model for the goals of the present paper.

The geometry shown in Fig. SI-2† was derived from the classical MD simulations in vacuum where Ru-POM is bound to graphene via two dendrimers (Fig. 3d). In this configuration Ru-POM is tightly wrapped by the organic ligands, hence we can expect the effect of the interaction with the support to be larger than the case of a single dendrimer. Rather than a realistic model of the molecule-substrate interface in solution, this geometry will therefore represent a worst-case scenario where the interaction with the support is maximized.

4.1 Initial state S_0: structural and electronic properties

The minimum energy structure and the electronic ground state calculated for the initial state S_0 of the Ru-POM supported by functionalized graphene are quite similar to the corresponding ones in vacuum. This is remarkable considering the tightly wrapped dendrimers around the molecular catalyst. The changes on the Ru-Ru distances in the tetrahedron core and the average of Ru-H_2O distances induced by the interaction with dendrimers/graphene are summarized in Table 1. This shows that the presence of the charged dendrimers around the Ru-POM molecule has a very limited effect on the structure of the core, and leads to slight distortions of the Ru_4O_6 core.

Table 1 Comparison of relative interatomic distances (in Å) in S_0 evaluated with / without MWCNT-dend. Ru1, Ru2 pair and Ru3, Ru4 pair cross the μ-hydroxo bridges, Ru1, Ru3 pair and Ru2, Ru4 pair cross the μ-oxo bridges.

	dend	vacuum[12]
d(Ru1,Ru2)	3.53	3.53
d(Ru3,Ru4)	3.55	3.54
d(Ru1,Ru3)	3.51	3.54
d(Ru2,Ru4)	3.54	3.54
d(Ru1,Ru4)	3.49	3.56
d(Ru2,Ru3)	3.48	3.56
$\bar{d}$(Ru,H_2O)	2.22	2.27

Not only the structural properties, but also the electron levels of the catalyst are not strongly affected by the interaction with the organic dendrimers and with the graphene surface. Similarly to the isolated case, also in the supported case the four Ru atoms are antiferromagnetically coupled across the μ-hydroxo bridge. The calculated density of states (DOS) and the projections (PDOS) are displayed in Fig. 6. The frontier orbitals in the PDOS clearly reveal that the highest occupied molecular orbital (HOMO) is related to Ru-POM molecule while the electronic states of all the other components (dendrimers and coronene) start appearing at energies 0.5 eV below the HOMO level. The calculated HOMO/LUMO (lowest unoccupied molecular orbital) gap is 0.30 eV, slightly lower than in vacuum (0.39 eV)[12]. More importantly, the PDOS in the lower panel in Fig. 6 demonstrates that the frontier orbitals are confined to the Ru_4O_6 core of the Ru-POM molecule, which was also the case for Ru-POM in vacuum[12]. Overall we conclude that the presence of the two dendrimers has no significant effects on the electronic properties of Ru-POM, even in the tight host-guest geometry predicted for the vacuum case.

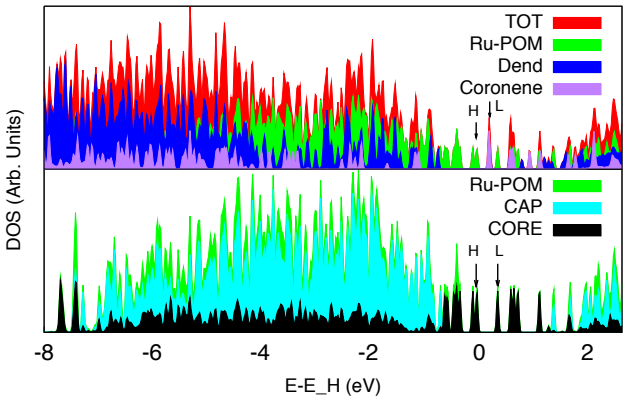

Fig. 6 Density of states for Ru-POM bound coronene via dendrimers (top panel) and for an isolated Ru-POM molecule (bottom panel). Total (red), and partial density of states (DOS) projected on Ru-POM complex (green), dendrimers (blue) and coronene molecules (purple) in the top panel, Ru-POM molecule (green), polyoxometalate ligands (cyan) and tetra ruthenium-oxo core (black) in the lower panel. The H and L labels indicate the HOMO and LUMO levels.

4.2 Higher oxidation states: S_1 - S_4

The water-oxidation energetics for the supported (red lines and numbers) and isolated (black lines and numbers) Ru-POM catalyst is reported in Fig. 7. By removing a proton and an electron from the initial state S_0 (PCET step), one of the water bound to a Ru center (Ru^{IV}-OH_2) is converted to a hydroxo ligand (Ru^{V}-OH, see S_1 intermediate in Figs. 5 and 7). The calculated free energy difference for this first PCET step is 0.65 eV for the supported and 0.57 eV for the vacuum case (Fig. 7). Similar small differences of less than 0.1 eV between supported and isolated catalyst are displayed for the other PCET steps leading to the S_2, S_3, and S_4 intermediates. Note that differences of 0.1 eV are within the accuracy of our calculations, particularly when comparing the results obtained with the same functional but with different basis sets and pseudopotentials. The overall free energy difference between S_0 and S_4 is 4.47 eV for the catalyst supported by

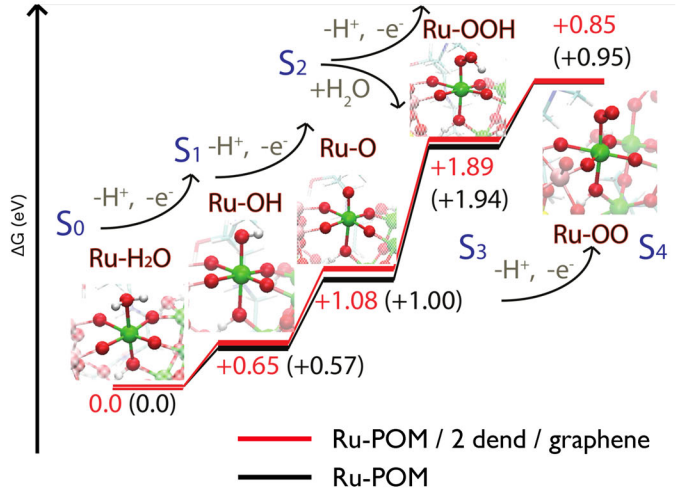

Fig. 7 Comparison of energetics of the intermediate states of oxidation between Ru-POM wrapped by dendrimers and Ru-POM in vacuum.

functionalized graphene and 4.46 eV for the vacuum case. In addition, this comparison shows that the energetic differences between the PCET steps in the two systems are not systematic.

The main result of this investigation, therefore, is that anchoring the Ru-POM catalyst to graphene via organic dendrimers does not alter the structural and electronic properties of the molecule, nor its ability to promote the oxidation of water. Note that these conclusions are based on simulations where we considered the functional groups tightly wrapped around Ru-POM, i.e. on a geometry obtained in vacuum. As we have shown, in solution the interaction between Ru-POM and the support is even weaker, with the dendrimers binding only to the POM caps of the molecule. We can therefore expect the effects of the support we calculated for the vacuum geometry to be even smaller for the solvated case.

5 Conclusions

In conclusion, we have parameterized and validated an atomistic empirical force field capable to capture the main interactions between the Ru-POM catalyst and a functionalized graphene electrode, both in vacuum and in solution. The MD simulations provide a detailed description of the interface geometry and interaction strength and show how these are extremely sensitive on the presence of the solvent. In vacuum the functional groups tightly wrap the Ru-POM molecule into a host-guest binding geometry and strongly anchor it to the graphene sheet. In solution the interaction is much weaker, the positively charged terminations of the dendrimers' branches spread out on the graphitic surfaces and bind the catalyst through one of its two POM terminations. In this binding geometry, all the Ru active sites of the Ru-POM catalyst are well exposed to the solvent.

The influence of the support on the structural and electronic properties on the catalyst is very small. In particular the free energy costs of a series of PCET steps that oxidize water to molecular oxygen differ by less than 0.1 eV when the catalyst is supported at the electrode or in vacuum. This small energy difference is below the accuracy of the present calculations.

This result provides a rational explanation for the similar Tafel slopes of the Ru-POM catalyst as measured in the homogeneous and heterogeneous phases.[14] We note however that the present study is limited to the description of thermodynamics and hence cannot explain the strong variation of the reaction rate (i.e. the turnover frequency at equal applied potential) for the Ru-POM catalyst supported by different substrates. For examples, the same experiments indicate that water oxidation by Ru-POM on graphene is about twice as fast as in the case of MWCNT and about ten times as fast as the homogeneous case.[14] The absolute reaction rate depends, among other things, on the electron transfer rate between the catalyst and the electrode. This charge injection is very sensitive to the geometry and to the electron leveling of the catalyst-electrode interface, which are very difficult to characterize experimentally. The detailed structural model of the interface provided by this study is therefore a necessary starting point for elucidating dynamical processes of charge injections at the electrode/catalyst so as to identify guidelines for increasing the absolute rate through interfacial structure and composition engineering.

6 Acknowledgement

We thank A. Sartorel, M. Bonchio, M. Prato, G. Scoles and G. Bussi for useful discussions. This work was partially funded by the EU through the FP7 Marie Curie IRG Program (Project H2OSPLIT, Grant PIRG04-GA-2008-239199). Computational resources were made available through PRACE Project H2OSPLIT (2010PA0315) and ENCORASOL (2012061002). SF acknowledges the financial support from the EU-FP7 COST action CM1104.

References

1 N. S. Lewis and D. G. Nocera, *Proc. Natl. Acad. Sci. U.S.A.*, 2005, **103**, 15729–15735.
2 V. Balzani, A. Credi and M. Venturi, *ChemSusChem*, 2008, **1**, 26–58.
3 H. Yamazaki, A. Shouji, M. Kajita and M. Yagi, *Coord. Chem. Rev.*, 2010, **254**, 2483–2491.
4 X. Sala, I. Romero, M. Rodríguez, L. Escriche and A. Llobet, *Angew. Chem., Int. Ed.*, 2009, **48**, 2842–2852.
5 N. Armaroli and V. Balzani, *Angew. Chem., Int. Ed.*, 2006, **46**, 52–66.

6 M. W. Kanan and D. G. Nocera, *Science*, 2008, **321**, 1072–1075.
7 M. Dinca, Y. Surendranath and D. G. Nocera, *Proc. Natl. Acad. Sci.*, 2010, doi: 10.1073/pnas.1001859107.
8 F. Jiao and H. Frei, *Energy Environ. Sci.*, 2010, **3**, 1018–1027.
9 F. Toma, A. Sartorel, M. Iurlo, M. Carraro and P. Parisse, *Nat. Chem.*, 2010, **2**, 826–831.
10 A. Sartorel, M. Carraro, G. Scorrano, R. De Zorzi, S. Geremia, N. D. McDaniel, S. Bernhard and M. Bonchio, *J. Am. Chem. Soc.*, 2008, **130**, 5006.
11 Y. V. Geletii, B. Botar, P. Kogerler, D. A. Hillesheim, D. G. Musaev and C. L. Hill, *Angew. Chem., Int. Ed.*, 2008, **47**, 3896–3899.
12 S. Piccinin and S. Fabris, *Phys. Chem. Chem. Phys.*, 2011, **13**, 7666–7674.
13 S. Piccinin, A. Sartorel, G. Aquilanti, A. Goldoni, M. Bonchio and S. Fabris, *Proc. Natl. Acad. Sci. U.S.A.*, 2013, **110**, 4917–4922.
14 M. Quintana, A. M. Lpez, S. Rapino, F. M. Toma, M. Iurlo, M. Carraro, A. Sartorel, C. Maccato, X. Ke, C. Bittencourt, T. Da Ros, G. Van Tendeloo, M. Marcaccio, F. Paolucci, M. Prato and M. Bonchio, *ACS Nano*, 2013, **7**, 811–817.
15 X. Ke, S. Turner, M. Quintana, C. Hadad, A. Montellano-Lpez, M. Carraro, A. Sartorel, M. Bonchio, M. Prato, C. Bittencourt and G. Van Tendeloo, *Small*, 2013, doi: 10.1002/smll.201300378.
16 P. E. Blöchl, *J. Chem. Phys.*, 1995, **103**, 7422.
17 J. Wang, R. Wolf, J. Caldwell, P. Kollman and D. Case, *J. Comp. Chem.*, 2004, **25**, 1157–1174.
18 D. J. Price and C. L. Brooks, *J. Chem. Phys.*, 2004, **121**, 10096.
19 S. Plimpton, *J. Compt. Phys.*, 1995, **117**, 1–19.
20 T. Darden, D. York and L. Pedersen, *J. Chem. Phys.*, 1993, **98**, 10089–10092.
21 X. López, C. Nieto-Draghi, C. Bo, J. B. Avalos and J. M. Poblet, *J. Phys. Chem. A*, 2005, **109**, 1216–1222.
22 C. Y. Tang and L. C. Zhang, *Nanotechnology*, 2004, **16**, 15–20.
23 G. Cicero, J. C. Grossman, E. Schwegler, F. Gygi and G. Galli, *J. Am. Chem. Soc.*, 2008, **130**, 1871–1878.
24 W. Cornell, P. Cieplak, C. Bayly, I. Gould, K. Merz, D. Ferguson, D. Spellmeyer, T. Fox, J. Caldwell and P. Kollman, *J. Am. Chem. Soc.*, 1995, **117**, 5179–5197.
25 Y. Duan, C. Wu, S. Chowdhury, M. Lee, G. Xiong, W. Zhang, R. Yang, P. Cieplak, R. Luo, T. Lee, J. Caldwell, J. Wang and P. Kollman, *J. Comp. Chem.*, 2003, **24**, 1999–2012.
26 G. Hummer, J. Rasaiah and J. Noworyta, *Nature*, 2001, **414**, 188–190.
27 H. Lee, J. R. Baker and R. G. Larson, *J. Phys. Chem. B*, 2006, **110**, 4014–4019.
28 P. K. Maiti and B. Bagchi, *Nano Letters*, 2006, **6**, 2478–2485.
29 B. Wu, B. Kerkeni, T. Egami, C. Do, Y. Liu, Y. Wang, L. Porcar, K. Hong, S. C. Smith, E. L. Liu, G. S. Smith and W.-R. Chen, *J. Chem. Phys.*, 2012, **136**, 144901.
30 A. Jakalian, D. B. Jack and C. I. Bayly, *J. Comp. Chem.*, 2002, **23**, 1623–1641.
31 J.-L. Li, K. Kudin, M. McAllister, R. Prud'homme, I. Aksay and R. Car, *Phys. Rev. Lett.*, 2006, **96**, 176101.
32 T. Sun and S. Fabris, *Nano Letters*, 2012, **12**, 17–21.
33 W. Kohn and L. Sham, *Phys. Rev.*, 1965, **140**, A1133–A1138.
34 J. Perdew, K. Burke and M. Ernzerhof, *Phys. Rev. Lett.*, 1996, **77**, 3865–3868.
35 D. Vanderbilt, *Phys. Rev. B*, 1990, **41**, 7892–7895.
36 P. Giannozzi, S. Baroni, N. Bonini, M. Calandra, R. Car, C. Cavazzoni, D. Ceresoli, G. Chiarotti, M. Cococcioni and I. Dabo, *J. Phys.: Condens. Matter.*, 2009, **21**, 395502.
37 J. K. Nørskov, J. Rossmeisl, A. Logadottir, L. Lindqvist, J. R. Kitchin, T. Bligaard and H. Jónsson, *J. Phys. Chem. B*, 2004, **108**, 17886–17892.
38 J. Rossmeisl, A. Logadottir and J. K. Nørskov, *Chem. Phys.*, 2005, **319**, 178–184.
39 J. Rossmeisl, J. K. Nørskov, C. D. Taylor, M. J. Janik and M. Neurock, *J. Phys. Chem. B*, 2006, **110**, 21833–21839.
40 J. Rossmeisl, Z. W. Qu, H. Zhu, G. J. Kroes and J. K. Nørskov, *J. Electroanal. Chem.*, 2007, **607**, 83–89.
41 J. M. Mayer, *Annu. Rev. Phys. Chem.*, 2004, **55**, 363–390.
42 D. R. Stull and H. Prophet, *JANAF Thermochemical Tables 2nd Edition*, U. S. National Bureau of Standards, Washington, DC, 1971.